1   **Re-investigating the coughing rat model of pertussis to understand *Bordetella pertussis***

2   **pathogenesis**

3

4   Jesse M. Hall[1,2], Jason Kang[1,2], Sophia M. Kenney[1,2], Ting Y. Wong[1,2], Graham J. Bitzer[1,2],

5   Claire O. Kelly[1,2], Caleb A. Kisamore[1,2], Dylan T. Boehm[1,2, *], Megan A. DeJong[1,2], M. Allison

6   Wolf[1,2], Emel Sen-Kilic[1,2], Alexander M. Horspool[1,2], Justin R Bevere[1,2], Mariette Barbier[1,2], &

7   F. Heath Damron[1,2, #]

8

9   [1] Department of Microbiology, Immunology and Cell Biology, School of Medicine, West

10   Virginia University, Morgantown, WV

11   [2] Vaccine Development Center, WVU Health Sciences Center, Morgantown, WV

12

13   Running title: Coughing rat model of pertussis

14

15   #Address correspondence to F. Heath Damron, fdamron@hsc.wvu.edu

16   *Present address: Vaccine and Gene Therapy Institute at Oregon Health Sciences University, 18

17   Beaverton, Oregon, USA

18

19

20

21

22

23

24

Abstract

Bordetella pertussis (*Bp*) is a highly contagious bacterium that is the causative agent of whooping cough (pertussis). Currently, acellular pertussis vaccines (aP; DTaP; Tdap) are used to prevent pertussis disease. However, it is clear that the aP vaccine efficacy quickly wanes, resulting in the re-emergence of pertussis. Furthermore, recent work performed by the CDC suggest that current circulating strains are genetically distinct from strains of the past. Emergence of genetically diverging strains combined with waning aP vaccine efficacy call for re-evaluation of current animal models of pertussis. In this study, we used the rat model of pertussis to compare two genetically divergent strains Tohama 1 and D420. We intranasally challenged seven-week-old Sprague-Dawley rats with 10^8 viable Tohama 1 and D420 and measured the hallmark signs/symptoms of *Bp* infection such as neutrophilia, pulmonary inflammation, and paroxysmal cough using whole body plethysmography. Onset of cough occurred between 2-4 days after *Bp* challenge averaging five coughs per fifteen minutes, with peak coughing occurring at day eight post infection averaging upward of thirteen coughs per fifteen minutes. However, we observed an increase of coughs in rats infected with clinical isolate D420 through 12 days post challenge. The rats exhibited increased bronchial restriction following *Bp* infection. Histology of the lung and flow cytometry confirm both cellular infiltration and pulmonary inflammation. D420 infection induced higher production of anti-*Bp* IgM antibodies compared to Tohama 1 infection. The coughing rat model provides a way of characterizing disease manifestation differences between *Bp* strains.

Introduction

Whooping cough (pertussis) is a respiratory disease that is caused by the bacterium *Bordetella pertussis (Bp)*. Pertussis is characterized by severe leukocytosis, bronchopneumonia, hypoglycemia, and paroxysmal cough (1, 2). During the catarrhal stage, *Bp* colonizes the upper respiratory epithelium. Once colonization occurs, *Bp* releases toxins such as pertussis toxin (PT), adenylate cyclase toxin (ACT) as well as others. Following the catarrhal stage is the paroxysmal stage that is characterized by severe coughing episodes. Innate and adaptive immune responses result in clearance of the bacterium allowing for the patient or host to convalescence. Despite extensive research, a full understanding of *Bp* pathogenesis remains elusive for reasons such as: vaccine pressure, lack of predictive models, and strain evolution (3). One of the major reasons for this gap of knowledge is the lack of a suitable animal model that shares common disease symptoms as seen in humans. Besides non-human primates, rats are the only other known model of pertussis that share similar coughing manifestation as seen in humans (4). As of now, the origin or the trigger of cough has yet to be determined (5). The rat model of pertussis offers a potential animal model that can be used to evaluate *Bp* pathogenesis.

In 1938, Hornibrook and Ashburn were the first to report that rats infected with *Bp* induced cough-like paroxysms and bronchopneumonia as seen in humans (6). Hornibrook and Ashburn found that young rats were capable of being infected and the bacterium could be cultured from the lungs (6). Infected rats produced coughs that could be heard from a distance of 20 feet (6). Twenty-six of the thirty-one infected rats that did not succumb to the infection had pathology indicative of inflammation in the lungs, most notably early neutrophil infiltration followed by recruitment of mononuclear cells (6). The subsequent studies utilized intrabronchial inoculation of *Bp* encased in

3

71   agar beads and confirmed leukocytosis and paroxysmal cough by sound activated tape recorders

72   from 5 to 21 days post challenge (7, 8). Further development of the rat model led to the evaluation

73   of PT negative strains and the evaluation of coughs (9). Strain BP357, which is deficient in PT

74   resulted in low cough induction (9). Further evaluation of the rat model demonstrated leukocytosis,

75   weight loss, and paroxysmal cough in Sprague-Dawley rats during the course of *Bp* infection (10).

76   During the development phase of the acellular pertussis vaccine (aP, DTaP), the rat model was

77   used to test vaccine efficacy of various acellular pertussis formulations and was used to validate

78   protection against the onset of leukocytosis and cough (11). Recently, an intranasal rat model has

79   been used to evaluate bacterial factors responsible for cough in *Bordetella bronchiseptica* (*Bb*)

80   (12). BspR ,which is an anti-sigma factor of *Bb*, plays some role in cough induction upon infection

81   (12). Collectively, these studies show that the pertussis rat model can be used to critically evaluate

82   *Bp* pathogenesis and disease progression.

83

84   In the 1940s, whole-cell pertussis (wP and DTP) vaccines were introduced to protect against *Bp*

85   infection (13). Widespread use of DTP in the United States led to a 90% decrease in the number

86   of reported *Bp* infections (13). Despite the efficacy of this vaccine, serious adverse side-effects

87   ensued, leading to the development of acellular pertussis vaccines. The antigens that are included

88   in the current aPs contain: filamentous hemagglutinin (FHA), fimbriae (FIM), PT, and pertactin

89   (PRN). After the switch from the wP to the aPs, there has been a significant increase in the number

90   of pertussis cases in the US and Europe (14). While nationwide vaccine coverage is 95% in the

91   United States, the incidence of *Bp* infections rose in the past 10 years as the number of aP

92   vaccinated only population has increased in size. (15). While vaccine coverage remains high, the

93   population dynamics are changing, and more people are aP immunized as the new generations are

94   born and as the wP only generations age. Numerous studies have demonstrated waning efficacy of

95   aPs in parallel with the emergence of genetically divergent strains of *Bp* (3, 16–21). Increased

96   surveillance of *Bp* has led to the identification of clinical isolates that do not express PRN, FIM,

97   and even PT the hallmark toxin of the organism (22). One plausible hypothesis to explain these

98   observations is that circulating *Bp* strains have evolved due to acellular vaccine pressure. While

99   we know the current strains are genetically different, we do not know if this genetic variability

100 affects virulence, disease burden, toxicity, or fitness of the pathogen (3).

101

102 Early rat studies were performed with intranasal administration of *Bp* for infection (6). Subsequent

103 rat challenge studies used *Bp* encased in agar beads for intrabronchial instillation (7–11, 23). While

104 the agar bead infection method was successful at establishing infection, we aimed to utilize the

105 simplicity of intranasal administration. We sought to re-investigate the coughing rat model of

106 pertussis to compare the pathogenesis of reference strain Tohama 1 to the recent clinical isolate

107 D420, which has been extensively studied in the baboon model of pertussis (24–30). Tohama 1

108 was first isolated from a case of whooping cough in 1954, while D420 was isolated in 2002 from

109 a critically ill infant in Texas (25, 31). Although Tohama 1 is now a reference strain that has been

110 widely used since Sato and Sato developed the aP but recent data has shown that this strain is an

111 considered an outlier (32, 33). Tohama 1 does expresses PRN but has lower expression of PT and

112 ACT (34). When Tohama 1 was used as a challenge strain in baboons, the baboons did not exhibit

113 symptoms of pertussis despite being infected (26). This led to the selection of recent clinical isolate

114 D420 as the baboon challenge strain, which readily infected and caused disease (26). With 48 years

115 of potential genetic divergence, we sought to understand the differences in pathogenesis between

116 these two commonly studied strains. D420 is known to infect mice and baboons and it belongs to

117   the clade (CDC013) of strains that represented 50% of isolates recovered in the US in 2000 (3).

118   However, it is important to note that D420 has an intact pertactin gene and it does express the PRN

119   protein as confirmed by shotgun proteomic analysis (data not shown).

120

121   In our current study, we aimed to re-establish an upper respiratory tract infection model in rats

122   following intranasal challenge with Tohama I and D420. We hypothesized that recent isolate D420

123   would induce a more severe disease profile compared to Tohama 1, as previous research

124   investigating pathogenesis in rhesus macaques noted that Tohama 1 infected animals did not

125   exhibit overt disease symptoms (26). Sprague-Dawley rats were intranasally challenged with *Bp*

126   and we characterized their disease progression profile over a twelve-day infection. Cough was

127   critically assessed utilizing whole body plethysmography (WBP). Bacterial colonization,

128   leukocytosis, and serological responses were measured as a result of infection. Rats challenged

129   with D420 had increased coughing, greater bacterial burden in the respiratory tract, and a more

130   robust IgM antibody response compared to Tohama 1. The coughing rat model of pertussis can

131   shed light on the pathogenesis of *Bp* and will likely be useful tool for pertussis vaccine evaluation.

132

133   **Results**

134   **D420 infected rats have increase number of coughs compared to strain Tohama 1 over the**

135   **entire course of infection.**

136   Over the past decade it is became clear that improvements to the acellular pertussis vaccine

137   strategy are needed due to the rise of PRN mutants, genomic divergence, and epidemiological data.

138   We believe in order to improve pertussis vaccines we need to better understand the pathogenesis

139   of *Bp* in an animal model that shares similar clinical manifestation of pertussis as seen in humans.

140   Here, we intranasally infected seven-week-old Sprague Dawley rats with 10^8 CFU of *Bp* strain

141   D420 or Tohama 1 (**Fig. 1**) in an effort establish infection and observe *Bp* induced cough. For

142   negative controls (no bacterial challenge), rats were intranasally administered sterile phosphate

143   buffer saline (PBS)**.** Paroxysmal cough is the hallmark symptom of pertussis and is thought to play

144   a major role in transmission of the organism to a new host. To quantify respiratory function during

145   infection, we utilized whole body plethysmography (WBP). WBP instrumentation consists of

146   specialized containment chambers which monitor box flow, temperature, and airflow changes to

147   measure respiratory function. Counting coughs via WBP provides an extremely accurate and

148   unbiased way of counting coughs based on cough waveforms. Rat containment chambers were

149   placed inside a laminar flow hood and connected to a computer that would monitor the rats

150   breathing (**Fig. S1**). Early studies reported that *Bp* infection in young rats induced coughs that were

151   audible by ear (6) and in our preliminary studies this was apparent to us as well (data not shown).

152   Studies in the 1990s, of paroxysmal cough in rats were quantified with an analog sound recording

153   device (7). We hypothesized that rats infected with recent isolate D420 would induce more coughs

154   than reference strain Tohama 1, because rhesus macaques infected with Tohama 1 did not exhibit

155   overt disease symptoms but D420 induced robust coughing in baboons (26). *Bp* infected rats

156   developed cough at days 2-11 (**Fig. 2B-C**), while the mock infected rats (**Fig. 2A**) only had a few

157   isolated coughs, unrelated to infection. Days 1-3 post infection, the average cough count of rats

158   infected with Tohama 1 or D420 was less then 5 coughs per fifteen minutes. The average cough

159   count doubled by day 7 post infection with peak coughing occurring at day 8 post infection with

160   an average of 13 coughs per fifteen minutes of monitoring. After day 8, the average cough count

161   for rats infected with D420 remained above 10 coughs per fifteen minutes, while the rats infected

162   with Tohama 1 averaged less then 5 coughs. To summarize the cough data, the average cough

7

163   count over the course of infection is shown **(Fig. 2D)**. We observed a significant increase in the

164   number of coughs at day eight post infection of *Bp* infected rats compared to the mock challenge

165   control. Rats infected with D420 coughed a total of 949 times, whereas rats infected with Tohama

166   1 coughed a total of 724 times over the entire twelve-day infection. To analyze differences in

167   cough count between strains, we utilized Area Under the Curve (AUC) analysis **(Fig. 2E)**. AUC

168   analysis allows us to quantify the number of coughs over the entire course of infection per rat.

169   Upon this analysis, we note a significant increase in the number of coughs for rats infected with

170   D420 compared to the mock challenged rats over the twelve-day infection, while there was no

171   significant difference observed in Tohama 1 infected rats compared to mock challenge (non-

172   infected).

173   ***Bp* infection causes pulmonary distress.**

174   Infection with *Bp* leads to mucus production, lung damage, and invasion of cellular infiltrates into

175   the bronchioles of the lung (35). The lungs of infants with *Bp* exhibit edema, necrotizing

176   bronchiolitis, and inflammation in the lung leading to respiratory distress (35). WBP was used to

177   quantify the pulmonary distress over the course of infection. Pulmonary distress was measured by

178   calculating the enhanced pause (PenH) of the animal (**Fig. 3A-B**). The higher the PenH value, the

179   increased respiratory distress of the animal. Compared to the mock challenged rats both D420 and

180   Tohama 1 infected rats had an increase in PenH (**Fig. 3A-B**). We observed a significant increase

181   at day 9 with rats infected with D420 and at day 6 with rats infected with Tohama 1 compared to

182   mock challenge.

183

184   **Histological assessment of the lung and nasal cavity**

185   To further evaluate the inflammation in the lung, we utilized histology to confirm both acute and

186   chronic inflammation in response to *Bp* infection. At days 1, 3, 6, 9, and 12 post challenge the left

187   lobes were collected, sectioned, and stained with hematoxylin and eosin (H&E) (**Fig. 4A&C**).

188   Whole-lung images were taken to assess cellular infiltration (**Fig. S2A&B**). Once stained, the

189   blinded slides were then scored by a board-certified pathologist. Mock challenge animals exhibited

190   minimal inflammatory infiltrates consisting of focal accumulations of mononuclear cells in the

191   parenchyma and occasional infiltrates of neutrophils surrounding blood vessels (**Fig. 4A**). Rats

192   infected with Tohama 1 and D420 had significant increase in their acute inflammation scores

193   compared to mock challenge animals at day 1 and 3 post infection (**Fig. 4B**). Day 1 post infection

194   had the highest acute inflammation score (**Fig. 4B**). Rats exhibited mild to moderate neutrophil

195   infiltration of the parenchyma, blood vessels, and the bronchioles (**Fig. 4A**). Markers of acute

196   inflammation resolved after day 6 post challenge; however, infected rats at day 9 exhibited obvious

197   differences in the lung associated with mild to moderate infiltration of mononuclear cells and

198   higher chronic inflammation compared to mock challenge animals (**Fig. 4C**). Interestingly, rats

199   infected with D420 had significant higher chronic inflammation score compared to rats infected

200   with Tohama 1 (**Fig. 4D**). At day 12 post infection, we notice moderate resolution of inflammation

201   in both D420 and Tohama 1 infected rats (**Fig. 4B&D**). We also observed a significant increase in

202   lung weight, which can also be associated with elevated inflammation, at days 1 and 9 post

203   challenge in D420 infected rats compared to the mock challenge control (**Fig. S3A**). At day 12

204   post challenge rats infected with Tohama 1 had a significant increase in lung weight compared to

205   the mock challenge rats (**Fig. S3A**). These results confirm that *Bp* infection induces inflammation

206   in the lung of coughing Sprague-Dawley rats.

207

208   Due to the fact that *Bp* is a mucosal pathogen, we sought out to investigate any phenotypic changes

209   or inflammation in the Nasal-Associated Lymphoid Tissue (NALT) of pertussis infected rats via

210   histology. NALT helps elicit immunity against airborne and mucosal pathogens (36). The NALT

211   is located above the hard palate and studies have also shown that with the introduction of antigen

212   via vaccination or bacterial components, cellular expansion of the NALT ensues (37–41). The

213   NALT was stained with H&E, and we observed an increase in cellular infiltrate and a size

214   enlargement in the NALTs of *Bp* infected rats compared to the mock challenged (**Fig. S4A**).

215   ImageJ analysis was used to measure the area of both the left and right NALT of each animal (**Fig.**

216   **S4B**). We observed a significant increase in the area of the NALT of rats infected with D420 at

217   day 6 and 9 compared to mock challenge, while we only saw an increase in the NALT area in

218   Tohama 1 infected rats at day 9 post challenge compared to our mock challenge control (**Fig. S4B**).

219   This data could mark the potential cellular expansion of the NALT upon infection with *Bp*. Further

220   analysis of the expanding cell populations in the NALT will warrant more analysis especially in

221   the context of vaccine immunity.

222   **D420 infected rats have increased bacterial burden in the respiratory tract.**

223   We determined bacterial burden in the respiratory tract for Tohama I and D420 challenged rats at

224   days 1, 3, 6, 9, and 12. Over the coughing timeline, we see an overall decrease in viable bacteria

225   in the lung, trachea, and nasal cavity. In the lung, we observed a significant increase in the

226   recovered bacteria in the D420 infected rats compared to the Tohama 1 infected rats at both days

227   3 and 6 (**Fig. 5A**). The same trend is also seen in the nasal cavity at day 1 post infection (**Fig. 5C**).

228   We observed no difference in the viable bacteria recovered in the trachea (**Fig. 5B**). Previous

229   pertussis studies utilizing the rat model of pertussis noted weight loss from intrabronchial infection

230   of *Bp* strain 18-323 (10). *Bp* infection is sufficient to cause weight loss in rats (10). To confirm

231 this using intranasal infection, body weight was measured before challenge and upon euthanasia

232 to calculate percent weight change. We observed a significant decrease in weight gain in rats

233 infected with *Bp* strain D420 and Tohama 1 compared to the mock challenged at day 12 post

234 infection (**Fig. S3B-D**). Next, we aimed to compare the bacterial colonization between outbred

235 mice and rats in an effort to relatively compare the bacterial burden between models. We utilized

236 the bacterial burden data in CD1 mice and compared them to our data in rats (42). To address the

237 body weight differences between the mice and rats, we used the CFUs/organ and divided them by

238 their respective body weight for a crude comparison. Our data suggests that despite having a higher

239 initial challenge dose in the rat, the bacterial burden remaining in the respiratory tract is higher in

240 a mouse compared to the rat later during infection (**Fig. S5**). In general, the rat model is likely a

241 lower challenge dose per body weight model of pertussis compared to mouse models.

242 **Immunofluorescence confirms colonization of *Bp* in the lungs and nasal cavity.**

243 We next wanted to assess the location of bacterial colonization in the nasal cavity and visualize

244 any bacteria left behind following flushing of the nares. We sectioned the skulls after flushing the

245 nasal cavity and utilized Immunofluorescence (IF). After visually scanning the nasal cavity with

246 confocal microscopy, we found bacteria in the nasal turbinates and the NALT (**Fig. 6A&C**). We

247 also confirmed that the bacteria were trapped in the crypts between the epithelial cells (**Fig. 6B**).

248 The relative locations of where the bacteria were found in the nasal cavity can be seen in (**Fig.**

249 **S6A**). Our results show that *Bp* remained in the nasal cavity over the entire course of infection

250 even after flushing the nares and the bacteria also remained captured in the cilia of the nasal

251 turbinates (**Fig. S6B**). The flushing of the nasal cavity underrepresents the total number of *Bp* in

252 the nasal cavity. In the lung, *Bp* colonizes the bronchioles, while the alveolar spaces remain non-

253 colonized (**Fig. 6D&F**). IF was performed on the nasal cavity and lung of mock challenge animals

11

254   to access non-specific binding (**Fig. S7**). To assess any potential differences between the strains

255   we blindly manually counted the labeled microcolonies in the lung and nasal cavity. It is also

256   worthy to note, we found no differences in microcolony counts in the lung or nasal cavity between

257   the strains (**Fig. S6 C-D**) despite our observed differences in bacterial burden by CFU

258   enumeration. CFU is likely a better indicator of overall bacterial burden, but IF revealed that *Bp*

259   is hiding and well attached in distinct locations in the airway.

260   **Measurement of recruitment of neutrophils in response to *Bp* infection**

261   Previous studies utilizing the rat model of pertussis noted leukocytosis and an increase in the

262   amount of total white blood cells using agar-encased *Bp* for infection (8). Neutrophils circulating

263   through the blood were measured during intranasal infection by antibody staining and flow

264   cytometry, as *Bp* infection results in varying amounts of neutrophilia (35, 43). The percentage of

265   CD45+ neutrophils in the blood were increased of infected rats compared to the mock challenged

266   animals (**Fig. 7A**). Specifically, a significant increase in the number of circulating neutrophils in

267   the blood of rats infected with D420 at days 1 and 9, with Tohama 1 infected rats only having a

268   significant increase to mock challenge at day 9 (**Fig. 7A**). Next, cytokines concentrations in the

269   lung and serum were measured to identify factors that could contribute to the recruitment of

270   neutrophils, specifically IL-6 and IL-17. IL-6 is a potent inducer of Th17 polarization and been

271   found elevated during murine infection with *Bp* (42, 44–46). Surprisingly, we did not observe any

272   significant changes in IL-6 due to *Bp* infection (**Fig. 7B&C**). It has been well documented in the

273   mouse model that the production of IL-17 in pertussis plays a role in the increase of circulating

274   neutrophils (47). There were no significant changes in IL-17a in the serum or lungs of *Bp* infected

275   rats compared to mock challenge (**Fig. 7D&E**). Th1 and Th2 cytokines and chemokines in the

276   lung and serum were also measured (**Fig. S7-Fig. S10**). We did not observe an increase in the

277   induction of cytokines by infection overall; however in the serum, rats infected with D420 had a

278   significant increase in IL-5 compared to Tohama 1 infected rats at day 12 post infection (**Fig. S8**).

279   There was a significant increase in IL-5 and TNF-alpha at day 6 post infection in the lung in rats

280   infected with Tohama 1 compared to D420 (**Fig. S9**). We also observed significant increases in

281   chemokines MIP-1a, RANTES, MCP-3, MIP-2, and IP10 in rats infected with D420 at day 12 post

282   challenge in the serum compared to rats infected with Tohama 1 (**Fig. S10**). In the lung, MIP-2

283   and IP10 were increased in rats infected with D420 compared to mock challenge control (**Fig.**

284   **S11**). Despite slight differences highlighted above we did not observe a massive difference in the

285   cytokine and chemokine responses during infection.

286   **Serological analysis of *Bp* specific antibodies**

287   Enzyme-linked immunosorbent assays (ELISA) were performed to determine the serological

288   response generated from *Bp* infection. We measured IgM and IgG antibody titers in the serum to

289   whole bacterium and *Bp* associated virulence factors at days 1, 3, 6, 9, and 12 post infection. In

290   previous studies utilizing the rat model, intrabronchial infection induced the generation of IgG

291   antibody titers to sonicated *Bp* 28 days post infection (8). Intranasal infection of strain D420 has

292   generated significant anti-PT IgG antibody titers in the baboon model at days 17-19 of infection

293   (26). However, analysis of antibody titers generated against an intranasal pertussis infection in the

294   rat has yet to be determined and we wanted to characterize the primary antibody response to *Bp*.

295   We observed a significant 10-fold increase in the anti-*Bp* IgM antibody response at day 9 and an

296   almost 20-fold increase 12 days post challenge in rats infected with D420 compared to mock

297   challenge, while we also saw a significant 6-fold increase in anti-*Bp* IgM at day 12 post infection

298   to the amount of anti-*Bp* IgM from Tohama 1 infection (**Fig. 8A&B**). At day 12 post infection, we

299   observed that *Bp* infection induced significant production of anti-*Bp* IgG in the serum compared

13

300   to mock challenge animals (**Fig. 8C&D**). At day 12 post infection, Tohama 1 infected rats had a

301   significant increase, nearly double anti-*Bp* IgG antibody titers compared to rats infected with

302   D420. AUC analysis revealed a significant increase in anti-*Bp* IgM antibodies from rats infected

303   with D420 compared to Tohama 1 infected rats (**Fig. S12A**). However, no difference was observed

304   in AUC of the anti-*Bp* IgG antibody response over the total course of infection between the

305   bacterial challenge groups (**Fig. S12B**). It is also important to note we also did not see a significant

306   increase in the generation of antibodies titers to PT, ACT, PRN, and FHA in *Bp* infected rats

307   compared to mock challenge infected animals (**Fig. 8A-D**). Graphs representing statistical

308   significance of the antibody titers between D420 and Tohama 1 infected rats can be observed in

309   the supplementary data (**Fig. S13**).

310   **<u>Discussion</u>**

311   To date, the only known reservoir for *Bp* is humans, making the development of a suitable animal

312   model challenging. Multiple models have been studied to recapitulate similar disease symptoms

313   seen in humans, as well as provide insight into the pathogenesis of *Bp*. We set out to re-investigate

314   the rat model of pertussis that was originally introduced in 1938 (6). In our study, we have

315   confirmed that intranasal administration of *Bp* led to bacterial colonization of the upper and lower

316   respiratory tract (**Fig. 5**). Through intranasal instillation, bacteria were able to infect the nasal

317   cavity, trachea, and lung post challenge. This is important to note as infants with pertussis

318   experience pneumonia more frequently than adolescents and adults (35). Mouse models of

319   pertussis also rely on depositing large numbers of bacteria into the lung to establish infection (2).

320   Here, our data shows that through intranasal infection, we establish an infection of both the upper

321   and lower respiratory tract, resembling the infection seen in adolescents and adults with pertussis.

322

323   Previous reports have shown *Bp* infection of rats induced paroxysmal coughs, and these coughs

324   were counted by analog audio recordings (7). Utilizing WBP we are able to precisely and digitally

325   count coughs and measure respiratory capacity for the first time with rats infected with *Bp* (**Fig.**

326   **2&3**). Here, coughs induced from infection appeared at day 1-2 post challenge, with the number

327   of coughs gradually increasing with peak cough occurring at day 8 post challenge. Rats challenged

328   with intrabronchial instillation of *Bp* noted similar peak cough counts approximately 10 days post

329   challenge (48). This is also one of the first studies utilizing WBP to count coughs in rats with

330   bacterial infection. We did observe some infected rats that did not overtly cough. This reflects the

331   frequency of coughs in adolescents and adults (49). Previous studies using baboons also show that

332   *Bp* infection elicits severe coughs lasting over 2 weeks post challenge with peak coughs per hour

333   being at day 4 post challenge (26). It is also important to note that at peak coughing, the bacterial

334   burden was low, which was also observed in previous *Bp* infected rat research (7). The data suggest

335   that other factors could be playing a role in cough production despite the bacterial infection being

336   resolved. We have also observed that the increased bronchi restriction coincides with the increased

337   coughs during days 6-11 post challenge (**Fig. 3**). The decreased lung capacity and increase in

338   cough could be further associated with an increase of chronic inflammation in the lung (**Fig. 4**).

339   Our data suggests that the coughing rat model of pertussis can be used to potentially evaluate the

340   mechanism of cough, which still requires further investigation.

341

342   Initial studies characterizing the serum antibody response to rats infected with *Bp* noted an increase

343   antibody response to endotoxin correlated with the low amount of cultivable organisms in the lung

344   following intrabronchial challenge (7). Hall et al. demonstrated that rats infected with *Bp* become

345   sera positive to whole cell *Bp* lysate, FHA, and PT at 28 days post intrabronchial challenge (8).

346   Anti-FHA antibody titers were not detected until day 16 post challenge, while anti-PT antibody

347   titers were not detected until day 28 post challenge (23). In our study, we characterized the

348   antibody response following intranasal challenge of *Bp* over the whole infection timeline. Using

349   *Bp* coated ELISA plates, we detected anti-*Bp* IgG antibody titers in rats infected with *Bp* at day 9

350   post challenge with a significant increase compared to mock challenge observed at day 12 (**Fig.**

351   **8**). We also measured a significant increase in anti-*Bp* IgM antibody titers in rats infected with

352   D420 compared to the mock challenge and Tohama 1 infected animals (**Fig. 8**). One potential

353   hypothesis that could explain this observation is the genetic differences between the two strains as

354   D420 harbors the *ptxP3* allele, leading to an increase in PT production (25). PT has been shown

355   to suppress *Bp* antibody responses in the serum and limit expression of antigen presenting

356   receptors (50–53).

357   With the increased interest in developing new pertussis vaccines, it is imperative for the

358   development of animal models to evaluate the pathogenic potential of current emerging strains, as

359   well as identify any potential differences in disease burden between genetically divergent strains.

360   Sato and Sato first used *Bp* strain Tohama 1 in the development of the acellular pertussis vaccine,

361   and Tohama 1 is still being used in pertussis research today, notably due to its genetic malleability

362   (54). D420 has been instrumental in the development of the baboon model and has also been used

363   to study vaccine efficacy in regards to transmission in the baboon model (29). In our study, we

364   observed multiple differences between Tohama 1 and D420 ranging from coughing, bacterial

365   colonization, and serological responses (**Fig. 2, 5, 8**). We hypothesize that these observed

366   differences could be due to the increased amount of PT through the *ptxP3* allele of D420 (25).

367   Strains, such as D420, harboring the *ptxP3* allele lead to increase in virulence, PT production, and

368   prevalence (55, 56). A previous study utilizing the intranasal mouse model has shown an increase

16

369 in bacterial colonization with *ptxP3* strains (57). Parton et al. illustrated that infection with a PT

370 deficient strain was unable to induce cough (9). It is possible that there are other factors beyond

371 PT that can account for the observed virulence differences between Tohama I and D420. In the

372 rat model, unlike the mouse, we also did not measure any significant increases in IL-17 and IL-6

373 in the lung and serum following challenge. IL-17 and IL-6 are increased following *Bp* infection in

374 mice and baboon (30, 44, 58). Further investigation is needed to explain the observed differences.

375

376 In summary, we have demonstrated that the rat model of pertussis can be used as a tool to further

377 study *Bp* pathogenesis and recapitulate some of the similar symptoms of pertussis as seen in

378 humans. Pertussis is often described as a 100 day cough, because adolescents and adults extended

379 duration of coughing (59). Coughing episodes in infants with pertussis can lead to vomiting,

380 choking, gagging, and apneic episodes that can lead to seizures (60). Mice have not been used to

381 evaluate coughing manifestation in pertussis until recently, and baboons are expensive and limited

382 to specialized facilities (61). The coughing rat of pertussis provides feasibility through low

383 husbandry costs, availability of animals, and ease of use as a model. In this study, we carefully

384 compared two established strains that have been used in the pertussis field, Tohama 1 and D420.

385 In future studies, we aim to evaluate whole cell and acellular vaccine mediated immunity against

386 D420. Armed with this model, we can further our understanding of pathogenesis, host response

387 during pertussis, genetic divergence between strains, and vaccine-mediated immunity.

388 **MATERIALS AND METHODS**

389 ***Bordetella pertussis* strains and growth conditions.** *Bp* strain Tohama 1 was graciously provided

390 by Dr. Peter Sebo (Czech Academy of Sciences) and strain D420 was acquired from the CDC

391 Pertussis Lab provided by Drs. Maria L. Tondella and Michael Weigand. *Bp* strain Tohama 1 and

17

392   D420 were cultured on Bordet Gengou (BG) agar (Remel^{TM} Cat. R45232) that was supplemented

393   with 15% defibrinated sheep blood (Hemostat Laboratories Cat. DSB500) (62). Bacteria were

394   cultured on BG plates for 48 hrs at 36°C. *Bp* was transferred from BG plates with polyester swabs

395   (Puritan Cat. 22-029-574) and transferred into 20 ml Stainer-Scholte liquid media (SSM) in new

396   125 ml flasks (Thermo Fisher Scientific Cat. FB500125) (63). The liquid cultures were grown for

397   24 hrs at 36°C inside a shaking incubator at 180 rpm.

398

399   **Intranasal challenge with *B. pertussis*.** Seven-week-old ~170g female Sprague-Dawley rats

400   (Charles River Cat. 001CD) were used for challenge. *Bp* was grown as described above. The rats

401   were then anesthetized with ketamine and xylazine 50-100/5-10 mg/kg and challenged with 10^8

402   CFUs (100µl intranasally), administering two 50µl doses one in each nostril (**Fig. 1**). Body weight

403   of each rat was recorded before challenge and immediately post euthanasia. Rats were euthanized

404   at day 1, 3, 6, 9, and 12 post bacterial challenge. Mock challenge animals (no bacteria) were

405   administered 100µl of sterile endotoxin free phosphate buffer saline (PBS) (Thermo Fisher

406   Scientific Cat. TMS012A) intranasally. Upon euthanasia blood was collected via cardiac puncture

407   and transferred into ethylenediaminetetraacetic acid (EDTA) (BD Cat. 365974) and serum

408   separation (BD Cat. 026897) tubes. Blood collected in the EDTA tube was used for flow

409   cytometric analysis, while blood collected int the serum separation tubes were used to isolate the

410   serum via centrifugation (15,000 x *g* for 3 min) and used for serological and cytokine analysis.

411   Lung and trachea were excised and homogenized to determine bacterial burden. Upon removal,

412   the wet weight of the lungs was recorded. Lungs were then collected in gentleMACS C tubes

413   (Miltenyi Biotec) and homogenized using gentleMACS™ Dissociator (Cat. 130-095-927). The

414   trachea was homogenized using a Polytron homogenizer. To determine the bacterial burden in the

18

415   nares, 2mls of sterile 1x PBS was flushed through the nares and collected for plating. Serial

416   dilutions of the homogenates and nasal collection were plated on BG plates supplemented with

417   ceftibuten (Sigma-Aldrich Cat. SML0037) 10 µg/ml to decrease growth of normal rat respiratory

418   tract flora.

419

420   **Analysis of coughing and bronchiole restriction using whole-body plethysmography.** To

421   quantify respiratory function during infection, we utilized a Buxco® FinePointe^{TM} Whole Body

422   Plethysmograph instrument (WBP) (DSI). FinePointe^{TM} software was used for collecting,

423   analyzing, and reporting the breathing data. Everyday post challenge for twelve consecutive days

424   at 5:00PM the rats were placed inside designated chambers to acclimate for 5 min. We chose this

425   time, not only due to rats being nocturnal, but this was the time the animals were most awake and

426   active as confirmed by video camera (data not shown). Following acclimation, the rat's respiratory

427   profile was recorded for 15 min. Each chamber is fitted with a transducer that measures the changes

428   in box flow and airflow of the subject. The chambers are also fitted with a screen pneumotach that

429   allows airflow in and out of the chamber that can be recorded. Coughs were counted during the

430   designated 15 min, and enhanced pause (PenH) was calculated to signify bronchiole restriction.

431   Coughs were counted based on large box flow changes of the subject, and changes in both humidity

432   and temperature of the air flowing in and out of the subject with classical cough-like waveforms.

433   Cough detection algorithm is applied with patented fuzzy logic criteria to determine if the event is

434   a cough (64). When analyzing the number of coughs, each cough in a multi-cough event was

435   counted individually.

436

437 **Histological assessment of the lung and nasal-associated lymphoid tissue.** Upon euthanasia,

438 the rat skull was excised, and the mandible removed. The skulls were fixed in 10% formalin (Fisher

439 Scientific Cat. SF98-4) for 48 hrs at 26 °C. After fixation, formalin was removed, and skulls were

440 frozen at -80 °C until decalcification. Skulls were de-calcified with Richard-Allan Scientific

441 decalcifying solution (Thermo Scientific Ref. 8340-1) at room temperature for 24-48 hrs and

442 embedded in paraffin. Samples were sectioned and stained with Hematoxylin-Eosin (H&E). A

443 Biotek Lionheart Fx was used to scan and image the NALT. ImageJ was used to trace and measure

444 the area of both the left and right NALT using the images from the Lionheart Fx. The left lobe of

445 the lung was excised and fixed in 10% formalin 48 hrs at 26 °C. The left lobe was then embedded

446 in paraffin and stained with H&E by the WVU Pathology Department. H&E stained sections were

447 used to characterize and score acute and chronic inflammation of the lung. All scorings were done

448 by a board-certified pathologist (iHisto). Individual scores were based on a standard qualitative

449 scoring criterion: (0 – none, 1 – minimal (rare), 2 – mild (slight), 3 – moderate, 4 – marked, 5 –

450 severe). Chronic inflammation was characterized by mononuclear infiltrates of the parenchyma,

451 blood vessels, and airway. Acute inflammation scores were assigned due to the presence of

452 neutrophils in the parenchyma, blood vessels, and airway. All examination and scoring were

453 performed blindly as no knowledge of treatment groups were known.

454

455 **Imaging of *Bp* in the lung and nasal cavity.** Detection of *Bp* in the nasal cavity and the lung were

456 quantified via immunofluorescence (IF) and confocal imaging. The left lobe of the lung and nasal

457 cavity were preserved and sectioned as described above. Sectioned samples underwent

458 deparaffination and rehydration using xylene and ethanol (100%-70%). Antigen retrieval was

459 performed by incubating samples in citrate buffer at 98 °C for 20 min. Samples were blocked using

20

460   5% Bovine Serum Albumin (BSA) (Fisher Scientific Cat. 159008) for 1 hr and primarily labeled

461   utilizing a polyclonal rabbit FHA antibody (Gift from Dr. Erik Hewlett) diluted in 1x PBS.

462   Secondary labeling occurred utilizing an anti-rabbit IgG conjugated with Texas Red (Fisher

463   Scientific Cat. T2767) diluted in 1x PBS. Samples were then covered in mounting media (Prolong

464   Gold Antifade reagent with DAPI Cat. 8961). Samples were imaged using a Nikon A1R confocal

465   microscope. Images were analyzed on DAPI channel and at wavelength 650nm for Texas-Red

466   acquisition. Images were acquired using 100x oil immersion lens (100x/1.40 Nikon Plan APO).

467   To identify any potential differences in IF between the two strains, all IF images were deidentified

468   and the microcolonies were manually counted blindly by four volunteers with 2-3 fields of view

469   used per sample.

470   **Flow cytometry analysis of phagocytes.** Neutrophil recruitment in the blood was evaluated by

471   flow cytometry. Blood samples upon collection were then lysed with Pharmylse buffer (BD

472   Biosciences Cat. 555899) for 20 min at room temperature, with slight vortexing throughout. The

473   remaining cells were centrifuged at 1,000 x g for 5 min and re-suspended in PBS + 1% fetal bovine

474   serum (FBS) (Gemini Bio Products Cat. 100-500) for 15 min on ice. Samples were then block with

475   anti-CD32 (BD Pharmingen Cat. 550270) antibody for 30 min at 4°C. After incubation, the cells

476   were stained with the appropriate antibody markers; CD45 Alexa flour 700 (Biolegend Cat.

477   202218), CD161 APC (Biolegend Cat. 205606), CD45R PE Cy7 (eBioscience Cat. 25-0460-82),

478   His48 FITC (eBioscience Cat. 11-0570-82), CD43 PE (Biolegend Cat. 202812), and CD3

479   VioGreen (Miltenyi Biotec Cat. 130-119-125) (65). After the addition of antibodies, the cells

480   incubated 1 hr at 4°C in the dark. To prepare the lung samples for flow cytometry, the lung

481   homogenate was pushed through a 70 µm cell strainer (BioDesign Cell MicroSives Cat. N70R),

482   creating a single-cell suspension. The suspension was centrifuged at 1,000 x g for 5 min. After

483   removal of the supernatant, the pellet was resuspended in Pharmlyse buffer and the cells incubated

484   at 37°C for 2 min. After incubation, the cells were centrifuged at 1,000 x g for 5 min, supernatant

485   was removed and blocked and labeled with antibody as described above. The lung and blood

486   samples were centrifuged at 1,000 x g for 5 min and the pellets were resuspended in 0.4%

487   paraformaldehyde and stored overnight at 4°C. Samples were washed with 1x PBS and

488   resuspended in 1x PBS for analysis. Cell samples were analyzed on a LSR Fortessa and samples

489   were gated and analyzed using FlowJo v10.

490   **Lung and serum cytokine and chemokine analysis.** Lung homogenate samples were centrifuged

491   at 19,000× g for 4 min and the supernatant was removed and stored at −80 °C. Quantitative

492   analysis of cytokines in the serum and lung homogenate was performed using ProcartaPlex

493   Multiplex Immunoassay kit: Cytokine & Chemokine 22-Plex Rat ProcartaPlex™ Panel (Cat.

494   EPX220-30122-901) per the manufacturer's instructions.

495

496   **Serological analysis.** Antibody titers of infected rats were measured by ELISA. *Bordetella*

497   *pertussis* specific ELISA plates were coated with 50 µl of 10^8 *B. pertussis* grown as mentioned

498   above for infection. For measurement of antibody titers to FHA (Enzo ALX-630-123-0100), PRN

499   (GSK), PT (List Biological Laboratories #180), and ACT (Gift from Dr. Erik Hewlett), we coated

500   plates with 50 µl of each antigen at 1µg/ml. Once coated, plates incubated over night at 4°C. Plates

501   were washed with 1x PBS-Tween 20 and blocked with 5% skim milk for 2 hours at 37°C. Plates

502   were washed again and the serum from the challenge studies were serially diluted down the ELISA

503   plate and incubated for 2 hours at 37°C. After incubation, the plates were washed and coated with

504   100µl of secondary goat anti-rat IgG (SouternBiotech Cat. 3030-04) and IgM (SouhternBiotech

505   Cat. 3020-04) antibody at a dilution of 1:2,000 in PBS + 5% milk. Once coated, the plate was

506   incubated for 1 hour at 37°C. Plates were then washed again with PBS-Tween 20 and 100 µl *p-*

507   nitrophenyl phosphate substate (Thermo Scientific Cat. 37620) was added, prepared by

508   manufactures instructions, and the plate was developed for 30 min at room temperature for titers

509   to IgG and IgM. Biotek Synergy H1 microplate reader was used to measure the colorimetric signal

510   of the ELISA plate at A_{450}. Positive antibody titers were determined by any values that were higher

511   than the baseline. The baseline is set as double the average value of the blank, no serum added to

512   these wells. Generating Nightingale rose plots in Python: Data from individual mice were averaged

513   in Microsoft Excel and log transformed. Values were formatted in Excel to be compatible with

514   Python. Data were imported from .csv files using the pandas package and plotted using the

515   "Barpolar" representation feature in the plotly.graph_objects module. Samples with a titer less

516   than 50 were assigned a value of 0.

517

518   **Statistical analysis.** All data was analyzed using GraphPad Prism 7. The minimum biological

519   replicates for the challenge studies were four. For statistical comparisons between multiple groups

520   over the entire course of the infection a two-way analysis of variance (ANOVA) was used One-

521   way ANOVA was used for comparison between groups for each individual day with Tukey's post

522   hoc test. Unpaired Student *t*-tests were used for area under the curve (AUC) analysis. Follow-up

523   statistical tests are annotated in figure legends.

524

525   **Data availability.** Data requests for figures provided can be addressed to the corresponding author.

526

527   **Ethics statement.** All studies were performed in accordance West Virginia University

528   Institutional Animal Care and Use Committee approved protocol 1811019148.6.

23

529 **ACKNOWLEDGMENTS**

539   JMH, DTB, and JK performed bacterial challenge. JMH, SMK, and JK monitored rat

540   coughing and respiratory function by whole body plethysmography. All authors participated in the

541   animal experiments. JMH and ESK contributed to flow cytometry panel design and analysis. JMH

542   and TYW prepared and ran flow cytometry samples. MAW and MAD performed cytokine

543   analysis. JMH analyzed H&E histology slides. JMH and GJB performed and analyzed

544   immunohistochemistry. JMH performed ELISA assays. JMH, MB, and FHD contributed to

545   experimental design. JMH wrote manuscript with critical revisions from all authors.

552   The authors would also like to acknowledge that figure 1 was Created with BioRender.com.

553

554 **References**

555 1.   Mattoo S, Cherry JD. 2005. Molecular pathogenesis, epidemiology, and clinical

556   manifestations of respiratory infections due to *Bordetella pertussis* and other *Bordetella*

557   subspecies. Clin Microbiol Rev 18:326–382.

558 2.   Melvin JA, Scheller E V., Miller JF, Cotter PA. 2014. *Bordetella pertussis* pathogenesis:

559   Current and future challenges. Nat Rev Microbiol2014/03/13. 12:274–288.

560 3.   Weigand MR, Peng Y, Loparev V, Batra D, Bowden KE, Burroughs M, Cassiday PK,

561   Davis JK, Johnson T, Juieng P, Knipe K, Mathis MH, Pruitt AM, Rowe L, Sheth M,

562   Tondella ML, Williams MM. 2017. The History of *Bordetella pertussis* Genome

563   Evolution Includes Structural Rearrangement. J Bacteriol 199:e00806-16.

564 4.   Elahi S, Holmstrom J, Gerdts V. 2007. The benefits of using diverse animal models for

565   studying pertussis. Trends Microbiol. Trends Microbiol.

566 5.   Cherry JD. 2015. The History of Pertussis (Whooping Cough); 1906–2015: Facts, Myths,

567   and Misconceptions. Curr Epidemiol Reports 2:120–130.

568 6.   Hornibrook JW, Ashburn LL. 1939. A Study of Experimental Pertussis in the Young Rat.

569   Public Heal Reports 54:439.

570 7.   Woods DE, Franklin R, Cryz SJ, Ganss M, Peppler M, Ewanowich C. 1989. Development

571   of a rat model for respiratory infection with *Bordetella pertussis*. Infect Immun 57:1018–

572   1024.

573 8.   Hall E, Parton R, Wardlaw AC. 1994. Cough production, leucocytosis and serology of rats

574   infected intrabronchially with *Bordetella pertussis*. J Med Microbiol 40:205–213.

25

575   9.   Parton R, Hall E, Wardlaw AC. 1994. Responses to *Bordetella pertussis* mutant strains

576   and to vaccination in the coughing rat model of pertussis. J Med Microbiol 40:307–312.

577   10.   Hall E, Parton R, Wardlaw AC. 1997. Differences in coughing and other responses to

578   intrabronchial infection with *Bordetella pertussis* among strains of rats. Infect Immun

579   65:4711–4717.

580   11.   Hall E, Parton R, Wardlaw AC. 1998. Responses to acellular pertussis vaccines and

581   component antigens in a coughing-rat model of pertussis. Vaccine 16:1595–603.

582   12.   Nakamura K, Shinoda N, Hiramatsu Y, Ohnishi S, Kamitani S, Ogura Y, Hayashi T,

583   Horiguchi Y. 2019. BspR/BtrA, an Anti-σ Factor, Regulates the Ability of *Bordetella*

584   *bronchiseptica* To Cause Cough in Rats. mSphere https://doi.org/10.1128/msphere.00093-

585   19.

586   13.   Libster R, Edwards KM. 2012. Re-emergence of pertussis: what are the solutions? Expert

587   Rev Vaccines 11:1331–1346.

588   14.   Hill HA, Elam-Evans LD, Yankey D, Singleton JA, Dietz V. 2016. Vaccination Coverage

589   Among Children Aged 19–35 Months — United States, 2015. MMWR Morb Mortal

590   Wkly Rep 65:1065–1071.

591   15.   National, State, and Local Area Vaccination Coverage Among Children Aged 19–35

592   Months — United States, 2011.

593   16.   Klein NP, Bartlett J, Fireman B, Baxter R. 2016. Waning Tdap Effectiveness in

594   Adolescents. Pediatrics.

595   17.   Klein NP, Bartlett J, Rowhani-Rahbar A, Fireman B, Baxter R. 2012. Waning Protection

596   after Fifth Dose of Acellular Pertussis Vaccine in Children. N Engl J Med 11367:1012–9.

597   18.   Klein NP, Bartlett J, Fireman B, Rowhani-Rahbar A, Baxter R. 2013. Comparative

598   Effectiveness of Acellular Versus Whole-Cell Pertussis Vaccines in Teenagers. Pediatrics

599   131:e1716–e1722.

600 19. Sheridan SL, Frith K, Snelling TL, Grimwood K, McIntyre PB, Lambert SB. 2014.

601   Waning vaccine immunity in teenagers primed with whole cell and acellular pertussis

602   vaccine: recent epidemiology. Expert Rev Vaccines 13:1081–1106.

603 20. Sheridan SL, Ware RS, Grimwood K, Lambert SB. 2012. Number and order of whole cell

604   pertussis vaccines in infancy and disease protection. JAMA - J Am Med Assoc. American

605   Medical Association.

606 21. Tartof SY, Lewis M, Kenyon C, White K, Osborn A, Liko J, Zell E, Martin S, Messonnier

607   NE, Clark TA, Skoff TH. 2013. Waning Immunity to Pertussis Following 5 Doses of

608   DTaP. Pediatrics2013/03/13. 131:e1047–e1052.

609 22. Williams MM, Sen KA, Weigand MR, Skoff TH, Cunningham VA, Halse TA, Tondella

610   ML. 2016. *Bordetella pertussis* strain lacking pertactin and pertussis toxin. Emerg Infect

611   Dis https://doi.org/10.3201/eid2202.151332.

612 23. Hall E, Parton R, Wardlaw AC. 1999. Time-course of infection and responses in a

613   coughing rat model of pertussis. J Med Microbiol 48:95–98.

614 24. Parkhill J, Sebaihia M, Preston A, Murphy LD, Thomson N, Harris DE, Holden MTG,

615   Churcher CM, Bentley SD, Mungall KL, Cerdeño-Tárraga AM, Temple L, James K,

616   Harris B, Quail MA, Achtman M, Atkin R, Baker S, Basham D, Bason N, Cherevach I,

617   Chillingworth T, Collins M, Cronin A, Davis P, Doggett J, Feltwell T, Goble A, Hamlin

618   N, Hauser H, Holroyd S, Jagels K, Leather S, Moule S, Norberczak H, O'Neil S, Ormond

619   D, Price C, Rabbinowitsch E, Rutter S, Sanders M, Saunders D, Seeger K, Sharp S,

620   Simmonds M, Skelton J, Squares R, Squares S, Stevens K, Unwin L, Whitehead S, Barrell

621   BG, Maskell DJ. 2003. Comparative analysis of the genome sequences of *Bordetella*

622   *pertussis, Bordetella parapertussis,* and *Bordetella bronchiseptica*. Nat Genet2003/08/12.

623   35:32–40.

624 25. Boinett CJ, Harris SR, Langridge GC, Trainor EA, Merkel TJ, Parkhill J. 2015. Complete

625   Genome Sequence of *Bordetella pertussis* D420. Genome Announc 3.

626 26. Warfel JM, Beren J, Kelly VK, Lee G, Merkel TJ. 2012. Nonhuman primate model of

627   pertussis. Infect Immun2012/01/19. 80:1530–1536.

628 27. Warfel JM, Merkel TJ. 2014. The baboon model of pertussis: Effective use and lessons for

629   pertussis vaccines. Expert Rev Vaccines 13:1241–1252.

630 28. Pinto M V., Merkel TJ. 2017. Pertussis disease and transmission and host responses:

631   insights from the baboon model of pertussis. J Infect 74:S114–S119.

632 29. Warfel JM, Zimmerman LI, Merkel TJ. 2014. Acellular pertussis vaccines protect against

633   disease butfail to prevent infection and transmission ina nonhuman primate model. Proc

634   Natl Acad Sci U S A 111:787–792.

635 30. Warfel JM, Merkel TJ. 2013. *Bordetella pertussis* infection induces a mucosal IL-17

636   response and long-lived Th17 and Th1 immune memory cells in nonhuman primates.

637   Mucosal Immunol 6:787–796.

638 31. KASUGA T, NAKASE Y, UKISHIMA K, TAKATSU K. 1954. Studies on *Haemophilus*

639   *pertussis*. V. Relation between the phase of bacilli and the progress of the whooping-

640   cough. Kitasato Arch Exp Med 27:57–62.

641 32. Caro V, Bouchez V, Guiso N. 2008. Is the Sequenced *Bordetella pertussis* strain Tohama

642   I representative of the species? J Clin Microbiol 46:2125–8.

643 33. Sato H, Sato Y. 1985. Protective antigens of *Bordetella pertussis* mouse-protection test

644   against intracerebral and aerosol challenge of *B. pertussis*. Dev Biol Stand 61:461–7.

645   34.   Barbier M, Boehm DT, Sen-Kilic E, Bonnin C, Pinheiro T, Hoffman C, Gray M, Hewlett

646   E, Damron FH. 2017. Modulation of pertussis and adenylate cyclase toxins by sigma

647   factor RpoE in *Bordetella pertussis*. Infect Immun 85.

648   35.   Paddock CD, Sanden GN, Cherry JD, Gal AA, Langston C, Tatti KM, Wu K, Goldsmith

649   CS, Greer PW, Montague JL, Eliason MT, Holman RC, Guarner J, Shieh W, Zaki SR.

650   2008. Pathology and Pathogenesis of Fatal *Bordetella pertussis* Infection in Infants. Clin

651   Infect Dis 47:328–338.

652   36.   Takaki H, Ichimiya S, Matsumoto M, Seya T. 2018. Mucosal Immune Response in Nasal-

653   Associated Lymphoid Tissue upon Intranasal Administration by Adjuvants. J Innate

654   Immun 10:515–521.

655   37.   Asanuma H, Hodson Thompson A, Iwasaki T, Sato Y, Inaba Y, Aizawa C, Kurata T,

656   Tamura S ichi. 1997. Isolation and characterization of mouse nasal-associated lymphoid

657   tissue. J Immunol Methods 202:123–131.

658   38.   Debertin AS, Tschernig T, Tönjes H, Kleemann WJ, Tröger HD, Pabst R. 2003. Nasal-

659   associated lymphoid tissue (NALT): frequency and localization in young children. Clin

660   Exp Immunol 134:503–507.

661   39.   Hirano T, Kodama S, Moriyama M, Kawano T, Suzuki M. 2009. The role of Toll-like

662   receptor 4 in eliciting acquired immune responses against nontypeable *Haemophilus*

663   *influenzae* following intranasal immunization with outer membrane protein. Int J Pediatr

664   Otorhinolaryngol 73:1657–1665.

665   40.   Petukhova G, Naikhin A, Chirkova T, Donina S, Korenkov D, Rudenko L. 2009.

666   Comparative studies of local antibody and cellular immune responses to influenza

667   infection and vaccination with live attenuated reassortant influenza vaccine (LAIV)

668   utilizing a mouse nasal-associated lymphoid tissue (NALT) separation method. Vaccine

669   27:2580–2587.

670   41.   Zuercher AW, Coffin SE, Thurnheer MC, Fundova P, Cebra JJ. 2002. Nasal-Associated

671   Lymphoid Tissue Is a Mucosal Inductive Site for Virus-Specific Humoral and Cellular

672   Immune Responses. J Immunol 168:1796–1803.

673   42.   Boehm DT, Hall JM, Wong TY, DiVenere A, Sen-Kilic E, Bevere JR, Bradford SD,

674   Blackwood CB, Elkins C, DeRoos KA, Gray MC, Cooper CG, Varney ME, Maynard JA,

675   Hewlett EL, Barbier M, Damron FH. 2018. Evaluation of adenylate cyclase toxoid antigen

676   in acellular pertussis vaccines using a *Bordetella pertussis* challenge model in mice. Infect

677   Immun IAI.00857-17.

678   43.   Sawal M, Cohen M, Irazuzta JE, Kumar R, Kirton C, Brundler M-A, Evans CA, Wilson

679   JA, Raffeeq P, Azaz A, Rotta AT, Vora A, Vohra A, Abboud P, Mirkin LD, Cooper M,

680   Dishop MK, Graf JM, Petros A, Klonin H. 2009. Fulminant pertussis: A multi-center

681   study with new insights into the clinico-pathological mechanisms. Pediatr Pulmonol

682   44:970–980.

683   44.   Boehm DT, Wolf MA, Hall JM, Wong TY, Sen-Kilic E, Basinger HD, Dziadowicz SA,

684   Gutierrez M de la P, Blackwood CB, Bradford SD, Begley KA, Witt WT, Varney ME,

685   Barbier M, Damron FH. 2019. Intranasal acellular pertussis vaccine provides mucosal

686   immunity and protects mice from *Bordetella pertussis*. npj Vaccines 4:1–12.

687   45.   Zhang X, Goel T, Goodfield LL, Muse SJ, Harvill ET. 2011. Decreased Leukocyte

688   Accumulation and Delayed *Bordetella pertussis* Clearance in IL-6-/- Mice. J Immunol

689   186:4895–4904.

690   46.   Wolf MA, Boehm DT, DeJong MA, Wong TY, Sen-Kilic E, Hall JM, Blackwood CB,

691   Weaver KL, Kelly CO, Kisamore CA, Bitzer GJ, Bevere JR, Barbier M, Damron FH.

692   2020. Intranasal immunization with acellular pertussis vaccines results in long-term

693   immunity to *Bordetella pertussis* in mice . Infect Immun IAI.00607-20.

694   47.   Andreasen C, Carbonetti NH. 2009. Role of neutrophils in response to *Bordetella*

695   *pertussis* infection in mice. Infect Immun2008/12/24. 77:1182–1188.

696   48.   Wardlaw AC, Hall E, Parton R. 1993. Coughing rat model of pertussis. Biologicals 21:27–

697   29.

698   49.   Kilgore PE, Salim AM, Zervos MJ, Schmitt H-J. 2016. Pertussis: Microbiology, Disease,

699   Treatment, and Prevention. Clin Microbiol Rev 29:449–86.

700   50.   Connelly CE, Sun Y, Carbonetti NH. 2012. Pertussis toxin exacerbates and prolongs

701   airway inflammatory responses during *Bordetella pertussis* infection. Infect Immun

702   80:4317–4332.

703   51.   Carbonetti NH, Artamonova G V, Andreasen C, Dudley E, Mays RM, Worthington ZE V.

704   2004. Suppression of Serum Antibody Responses by Pertussis Toxin after Respiratory

705   Tract Colonization by *Bordetella pertussis* and Identification of an Immunodominant

706   Lipoprotein. Infect Immun 72:3350–3358.

707   52.   Shumilla JA, Lacaille V, Hornell TMC, Huang J, Narasimhan S, Relman DA, Mellins ED.

708   2004. *Bordetella pertussis* Infection of Primary Human Monocytes Alters HLA-DR

709   Expression. Infect Immun 72:1450–1462.

710   53.   Martino A, Volpe E, Auricchio G, Colizzi V, Baldini PM. 2006. Influence of Pertussis

711   toxin on CD1a isoform expression in human dendritic cells. J Clin Immunol 26:153–159.

712   54.   Weiss AA, Falkow S. 1982. Plasmid Transfer to *Bordetella pertussis*: Conjugation and

713   Transformation Downloaded from JOURNAL OF BACTERIOLOGY.

714 55. Mooi FR, Van Loo IHM, Van Gent M, He Q, Bart MJ, Heuvelman KJ, De Greeff SC,

715   Diavatopoulos D, Teunis P, Nagelkerke N, Mertsola J. 2009. *Bordetella pertussis* strains

716   with increased toxin production associated with pertussis resurgence. Emerg Infect Dis

717   15:1206–1213.

718 56. Advani A, Gustafsson L, Carlsson RM, Donnelly D, Hallander HO. 2007. Clinical

719   outcome of pertussis in Sweden: Association with pulsed-field gel electrophoresis profiles

720   and serotype. APMIS 115:736–742.

721 57. King AJ, Van Der Lee S, Mohangoo A, Van Gent M, Van Der Ark A, Van De

722   Waterbeemd B. Genome-Wide Gene Expression Analysis of *Bordetella pertussis* Isolates

723   Associated with a Resurgence in Pertussis: Elucidation of Factors Involved in the

724   Increased Fitness of Epidemic Strains https://doi.org/10.1371/journal.pone.0066150.

725 58. Andreasen C, Powell DA, Carbonetti NH. 2009. Pertussis toxin stimulates IL-17

726   production in response to *Bordetella pertussis* infection in mice. PLoS One 4:e7079.

727 59. Lee GM, Lett S, Schauer S, Lebaron C, Murphy T V, Rusinak D, Lieu TA. 2004. Societal

728   Costs and Morbidity of Pertussis in Adolescents and Adults.

729 60. Cherry JD. 2016. Pertussis in young infants throughout the world. Clin Infect Dis

730   63:S119–S122.

731 61. Hiramatsu Y, Suzuki K, Nishida T, Onoda N, Satoh T, Akira S, Ikawa M, Ikeda H, Kamei

732   J, Derouiche S, Tominaga M, Horiguchi Y. 2020. Lipooligosaccharide, Vag8, and

733   pertussis toxin of *Bordetella pertussis* cooperatively cause coughing in mice. bioRxiv.

734   bioRxiv.

735 62. Bordet J, Gengou O. 1906. Le Microbe de la Coqueluche. Les Ann l'Institut Pasteur

736   20:731–741.

737   63.   Stainer DW, Scholte MJ. 1970. A Simple Chemically Defined Medium for the Production

738   of Phase I *Bordetella pertussis*. J Gen Microbiol1970/10/01. 63:211–220.

739   64.   Lomask J, Larson R. 2006. United States Patent USOO7104962B2. US 7,104,962 B2.

740   65.   Barnett-Vanes A, Sharrock A, Birrell MA, Rankin S. 2016. A Single 9-Colour Flow

741   Cytometric Method to Characterise Major Leukocyte Populations in the Rat: Validation in

742   a Model of LPS-Induced Pulmonary Inflammation

743   https://doi.org/10.1371/journal.pone.0142520.

744

745   **FIGURES**

Figure 1:
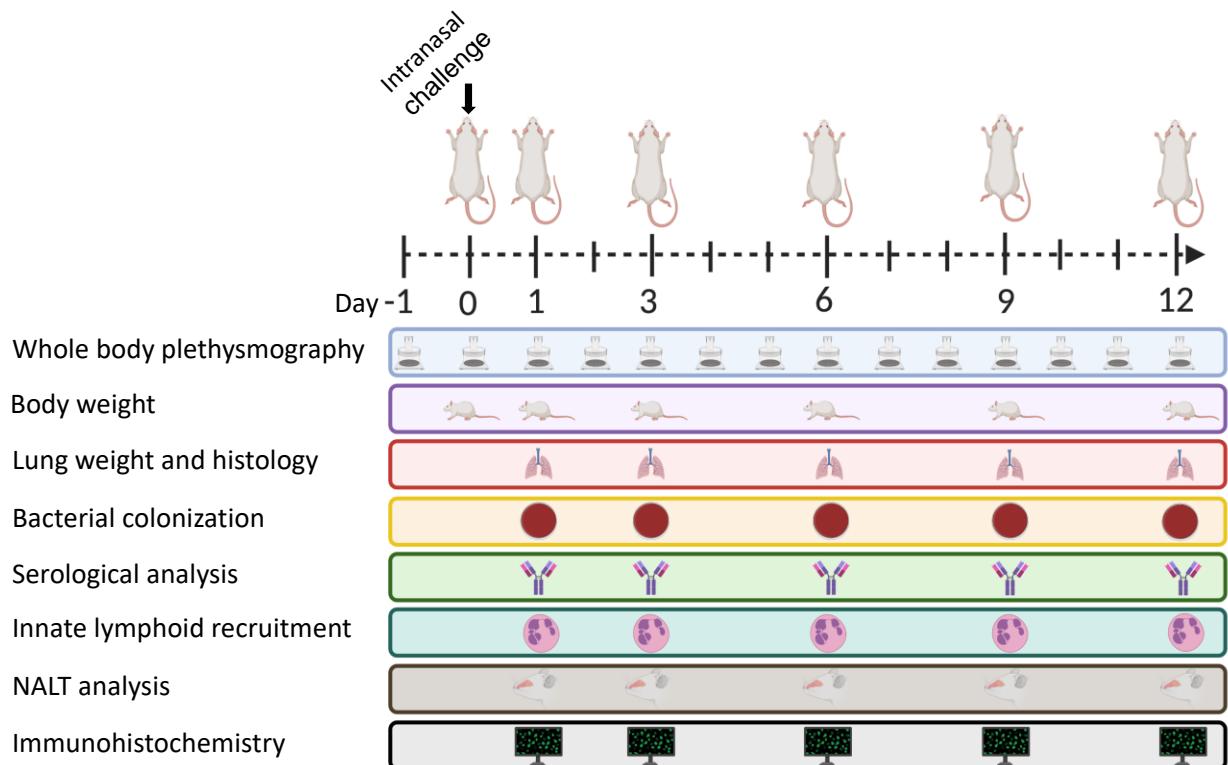
746 **FIG 1** Experimental design of intranasal infection of *Bp*. Schematic representation of Sprague-

747 Dawley rats intranasally infected with *Bp*. Whole body plethysmography was used to measure

748 cough and analyze lung function over the course of a twelve-day infection. Body weight, Bacterial

749 burden of the respiratory tract, innate lymphoid recruitment, and antibody titers were measured at

750 the days 1, 3, 6, 9, and 12 post challenge. The left lobe of the lung and NALT were sectioned and

751 stained with hematoxylin and eosin for histological analysis and immunohistochemistry was

752 performed to visualize bacteria in the left lobe of the lung and nasal cavity.

Figure 2:
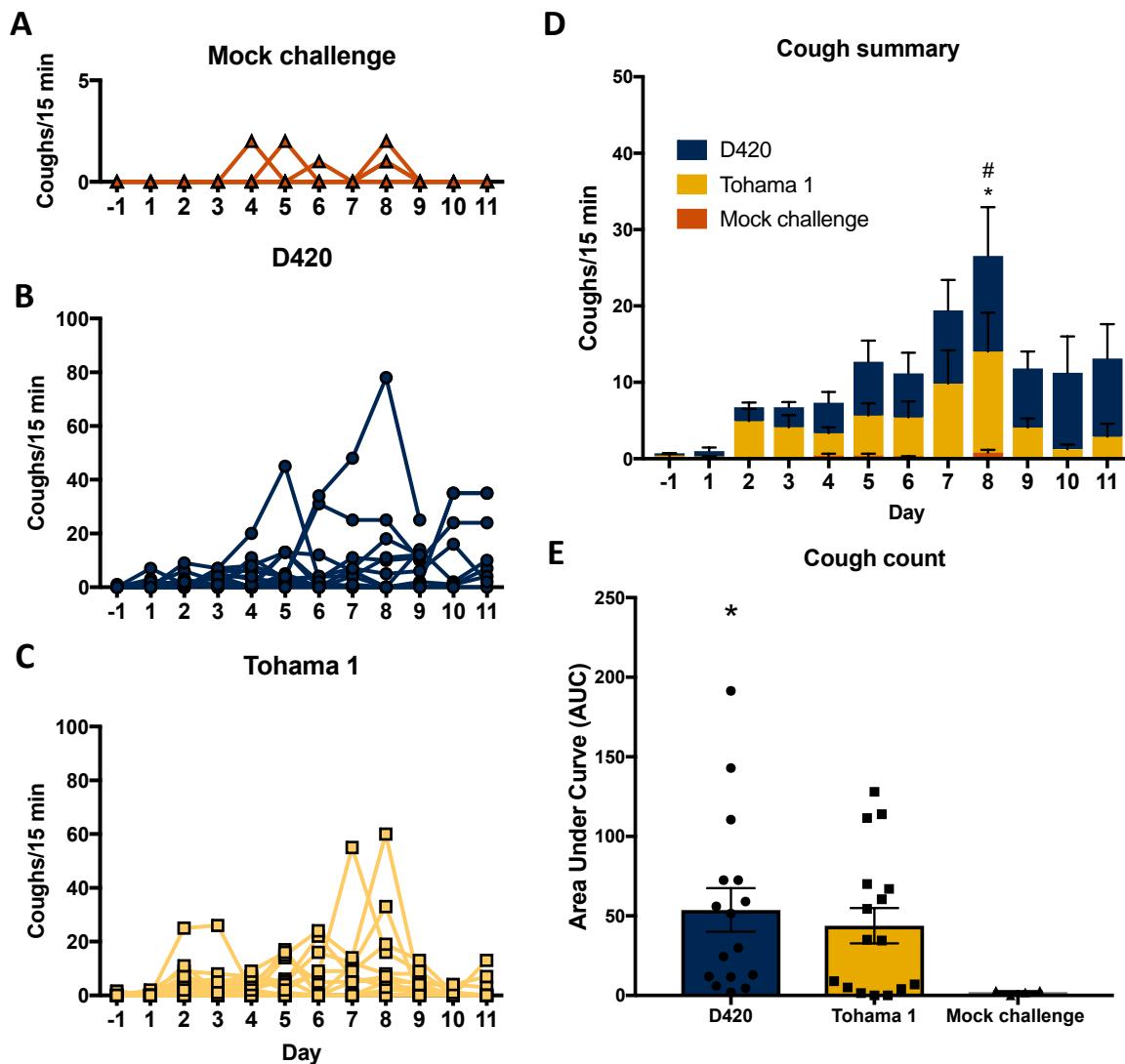
FIG 2 Infection of *Bordetella pertussis* induces cough in Sprague-Dawley rats. Coughs were measured each day of the twelve-day infection using whole body plethysmography. Coughs were counted for (A) mock challenge rats, (B) rats infected with D420, and (C) rats infected with Tohama 1. (D) Summary of results (A-C) shown as mean ± SEM (n = 4-8). (E) Area under the curve is represented as averages of coughs per fifteen minutes for each rat. *P* values were determined by two-way ANOVA followed by a Bonferroni comparison test and unpaired Student

35

759   t-test for AUC, $*P < 0.05$ D420 compared to the mock challenged control group, $^{\#}P < 0.05$ Tohama

760   1 compared to the mock challenged control group.

Figure 3:
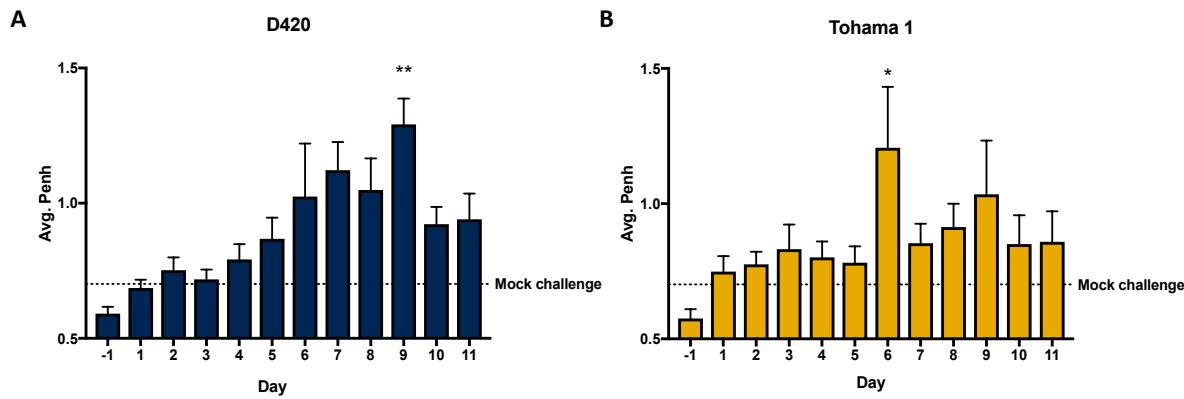
761   **FIG 3** *Bordetella pertussis* infection impairs respiratory capacity. Over the course of infection,

762   Sprague-Dawley rat's respiratory function was analyzed using whole body plethysmography. Each

763   day at 5p.m., rat's bronchial restriction was determined by utilizing WBP by calculating for PenH.

764   Penh was calculated **for (A)** D420 and **(B)** Tohama 1. Results shown as mean $\pm$ SEM ($n = 4$-

765   8). *P* values were determined by two-way ANOVA, $*P < 0.05$, $**P < 0.01$ compared to the mock

766   challenge group followed by Dunnett's comparison test.

36

Figure 4:
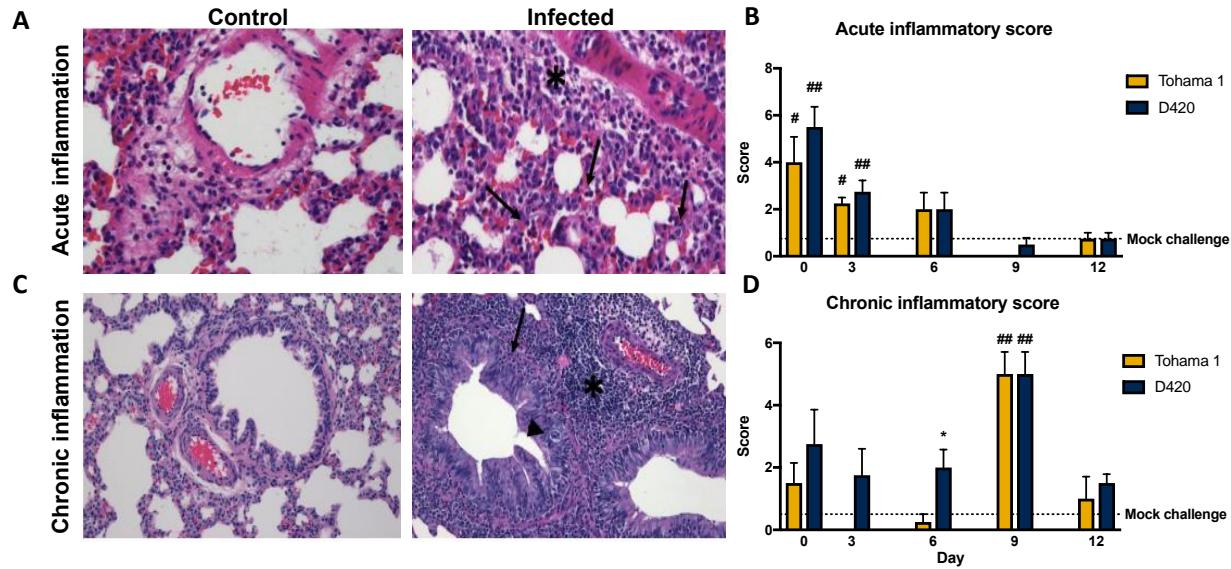
FIG 4 *Bordetella pertussis* infection induces acute and chronic inflammation in the lung of Sprague-Dawley rats. The left lobe of the lung was sectioned and stained with hematoxylin and eosin from rats infected with D420, Tohama 1, or the PBS control. **(A)** Representative images of acute inflammation demonstrating neutrophil recruitment around surrounding blood vessel (asterisk) and parenchyma (arrows) at 400x magnification. **(B)** Average acute inflammatory score of the lung by the predominance of neutrophils in the parenchyma, blood vessels, and airways. **(C)** Representative images of chronic inflammation showing mononuclear cells surrounding the blood vessel (asterisk), lamina propria (arrow), and bronchioles (arrowhead) at 200x magnification. **(D)** Average chronic inflammatory score of the lung characterized by mononuclear infiltrates in the parenchyma, blood vessels, and airway. Histological assessment was determined blinded with no knowledge of the treatment groups. Results are shown as mean $\pm$ SEM ($n = 4$) P values were determined by one-way ANOVA followed by Dunnett's comparison test, $*P < 0.05$ compared between challenge groups. $^{\#}P < 0.05$, $^{\#\#}P < 0.01$ compared to mock challenge.

37

Figure 5:
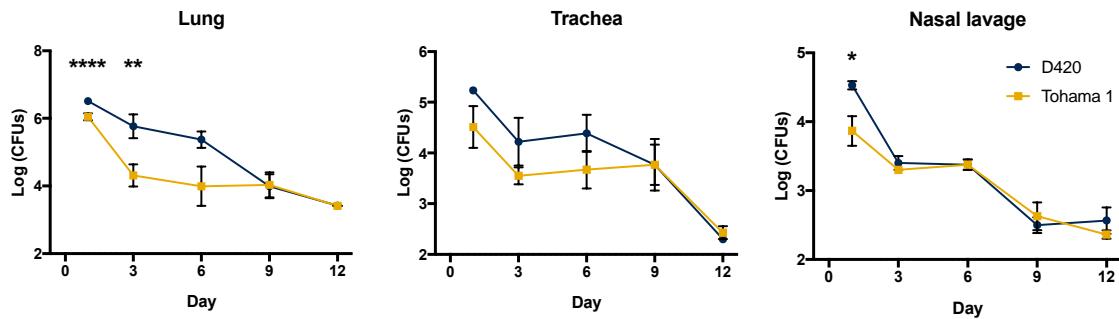
780   **FIG 5** Analysis of bacterial burden over the course of *Bp* infection. Bacteria were quantified by

781   serially diluted CFUs following intranasal challenge. CFU counts were determined from **(A)** lung

782   homogenate **(B)** trachea and **(C)** nasal lavage. Results are shown as mean $\pm$ SEM ($n = 4$) *P* values

783   were determined by two-way ANOVA corrected with Bonferroni comparison test, *$P < 0.05$,

784   **$P < 0.01$, ****$P < 0.0001$ compared between D420 and Tohama 1.

785

Figure 6:
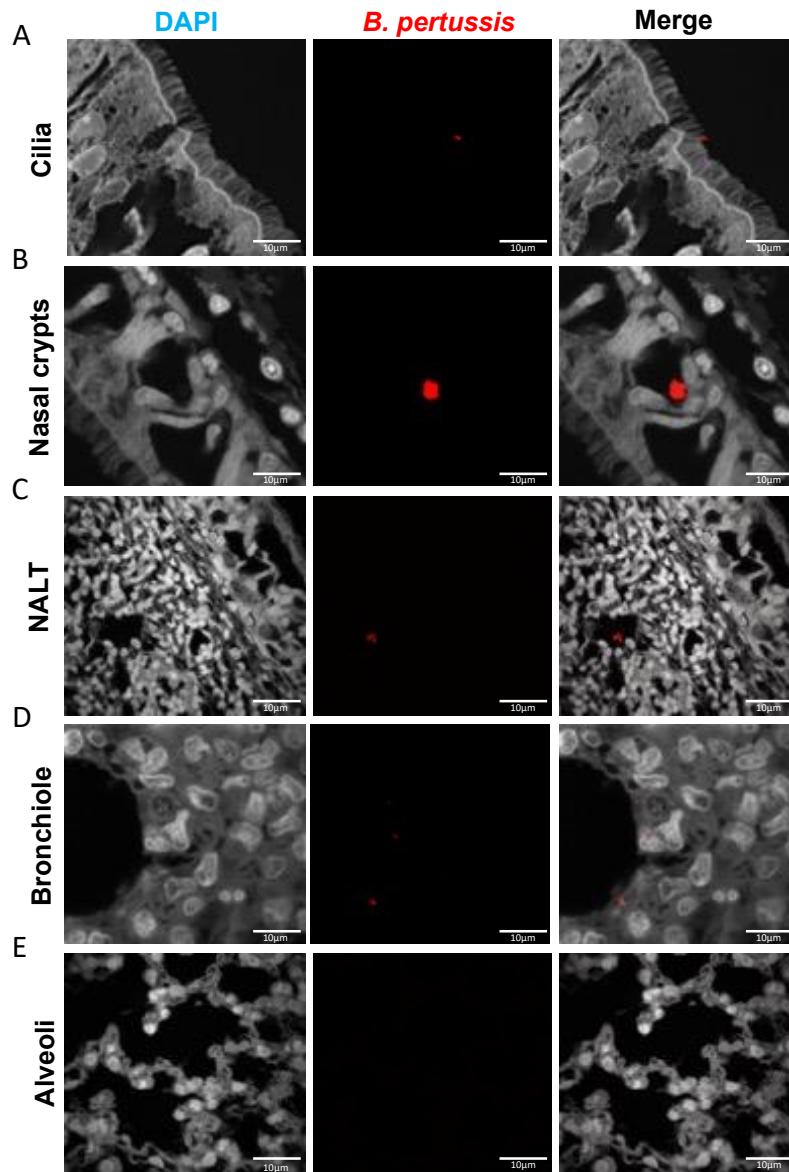
786   **FIG 6** Immunofluorescence (IF) staining of *Bp* localization in the respiratory tract. *Bp* was labeled

787   using a polyclonal antibody to FHA and counter tagged with a fluorescently conjugated antibody

788   (Texas-Red). Sections were counterstained with DAPI. **(A-C)** Representative images of *Bp* in the

789   nasal cavity over the course of infection. *Bp* was found captured in the cilia of the nasal cavity as

790 well as the NALT. **(D-E)** Representative images of the bronchiole and alveoli of infected rats. *Bp*

791 was found localized in the bronchioles over the course of infection and absent in the alveoli.

Figure 7:
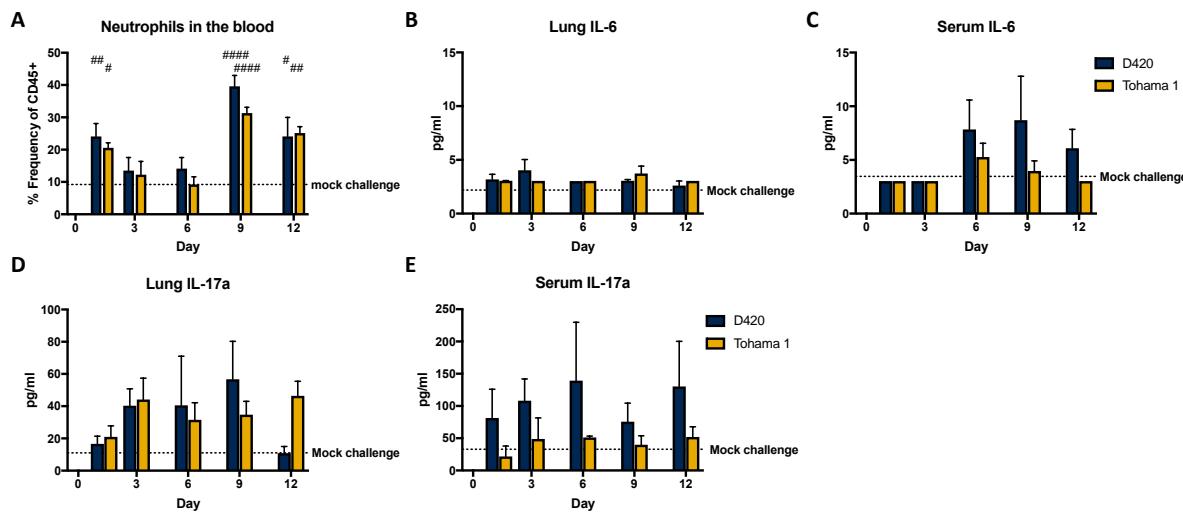
792 **FIG 7** Neutrophil recruitment and proinflammatory cytokine production after challenge

793 determined by flow cytometry and multiplex immunoassay analysis. **(A)** Blood neutrophil count

794 of Sprague-Dawley rats infected with *Bp*. At days 1, 3, 6, 9 and 12 post infection, rats were

795 euthanized, and the blood was collected via cardiac puncture. Flow cytometry was used to quantify

796 the amount of neutrophils (CD45$^+$ CD161$^-$ B220$^-$ CD43$^+$ His48^{hi}) in the blood. Quantification of

797 the percentage of single, CD45+ cells. Dotted line represents the average frequency of CD45+

798 neutrophils in the mock challenge animals over the course of the study. **(B-C)** Analysis of cytokine

799 IL-6 from supernatant of lung homogenate and serum. **(D-E)** analysis of cytokine IL-17 in the

800 serum and lung homogenate supernatant. Cytokines analyzed using ProcartaPlex multiplex

801 immunoassay kit. Results shown as mean $\pm$ SEM ($n = 4$). Dotted line represents the average mock

802 challenged cytokine levels measured. *P* values were determined by one-way ANOVA followed by

803 Tukey comparison test, $^{\#}P < 0.05$, $^{\#\#}P < 0.01$, $^{\#\#\#\#}P < 0.0001$ compared to mock challenge.

Figure 8:
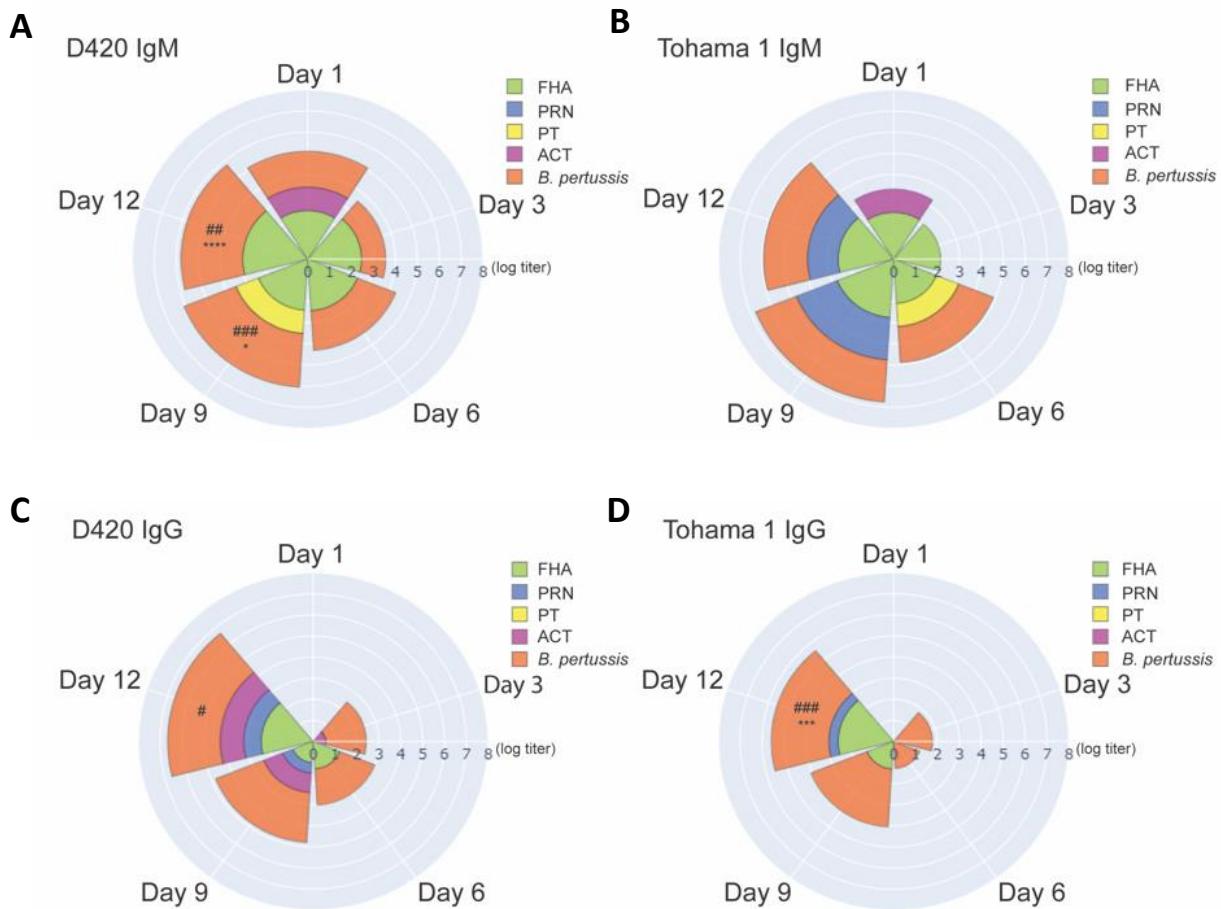
FIG 8 Measurement of serum antibody titers over the course of *Bp* infection. ELISA was used to compare serological responses from rats IN challenge with *Bp*. Total IgM (A-B) and IgG (C-D) serum antibody titers were measured from challenged rats against *Bp*, FHA, PRN, PT, and ACT. ($n = 4$). *P* values were determined by two-way ANOVA corrected with Bonferroni comparison test, $*P < 0.05$, $***P < 0.001$, $****P < 0.0001$ compared between infection groups. For comparison to mock challenged control group one-way ANOVA was used followed by Tukey comparison test, $^{\#}P < 0.05$, $^{\#\#}P < 0.01$, $^{\#\#\#}P < 0.001$.

41